Salmonella typhimurium Lacking Ribose Chemoreceptors Localize in Tumor Quiescence and Induce Apoptosis

Rachel W. Kasinskas and Neil S. Forbes

Department of Chemical Engineering, University of Massachusetts at Amherst, Amherst, Massachusetts

Abstract

The effectiveness of most chemotherapeutics is limited by their inability to penetrate deep into tumor tissue and their ineffectiveness against quiescent cells. Motile *Salmonella typhimurium*, which are specifically attracted to compounds produced by quiescent cancer cells, could overcome this therapeutic barrier. We hypothesized that individual chemoreceptors target *S. typhimurium* to specific tumor microenvironments. To test this hypothesis, we used time-lapse fluorescent microscopy and tumor cylindroids to quantify the accumulation of chemotaxis machinery knockouts, including strains lacking individual cell surface chemoreceptors, chemotaxis signal transduction pathway enzymes, and the flagella and motor assemblies. To measure the extent of apoptosis induced by individual bacterial strains, caspase-3 activity was measured as a function of time. Our results showed how chemoreceptors directed bacterial chemotaxis within cylindroids: the aspartate receptor initiated chemotaxis toward cylindroids, the serine receptor initiated penetration, and the ribose/galactose receptor directed *S. typhimurium* toward necrosis. In addition, strains lacking proper flagella constructs, signal transduction proteins, or active motor function did not chemotax toward tumor cylindroids, indicating that directed chemotaxis is necessary to promote accumulation in tumors. By deleting the ribose/galactose receptor, bacterial accumulation localized to tumor quiescence and had a greater individual effect on inducing apoptosis than wild-type *S. typhimurium*. This new understanding of the mechanisms of Salmonella migration in tumors will allow for the development of bacterial therapies with improved targeting to therapeutically inaccessible regions of tumors. [Cancer Res 2007;67(7):3201–9]

Introduction

Motile, nonpathogenic bacteria have the potential to overcome multidrug resistance (1) because they can penetrate deeper than passively diffusing drug molecules (2–5). Multidrug resistance, which significantly reduces the effectiveness of most cancer therapeutics, is caused by two mechanisms: limited drug penetration and poor cell susceptibility (6, 7). Uneven perfusion in tumors creates populations of cells that are physically distant from therapeutics in the bloodstream and are quiescent due to nutrient deficiencies (8). Motile facultative anaerobes, which include *Salmonella typhimurium*, have the potential to actively penetrate into tumor tissue and overcome diffusion limitations, where they could attack quiescent cancer cells that are impervious to standard chemotherapies. Because of the importance of intratumoral targeting, understanding bacterial motility in tumors is a critical step in the development of effective bacterial therapies.

To date, the mechanisms that control bacterial motility in tumors are poorly understood. Recently, we have shown that (*a*) *S. typhimurium* accumulate within the necrotic regions of both *in vitro* and *in vivo* tumors, (*b*) chemotaxis is essential to initiate accumulation, and (*c*) preferential proliferation enhances region-specific accumulation at longer times (1, 5). Our group and others showed that nonpathogenic *S. typhimurium* (9–11) retard tumor growth, prolong survival in mice (3, 9, 10, 12, 13), and preferentially accumulate 2,000-fold more in tumors than in liver, spleen, lung, heart, and skin (5, 14). Hoffmann et al. (15, 16) have created a *S. typhimurium* mutant auxotrophic strain for leucine and arginine that preferentially proliferates throughout tumors and causes regression of human prostate tumors in mice. We believe that understanding chemotaxis is essential for controlling *S. typhimurium* targeting in tumors.

We hypothesized that individual chemoreceptors target *S. typhimurium* to specific regions of tumors by controlling their chemotaxis toward specific tumor microenvironments. We also hypothesized that *S. typhimurium* targeted to quiescence induce apoptosis in cylindroids. To test these hypotheses, we used time-lapse fluorescent microscopy to quantify the accumulation pattern of a series of chemotaxis machinery knockouts in tumor cylindroids. Cylindroids are an *in vitro* tumor model developed in our laboratory to mimic the microenvironments and metabolite gradients in human tumors (1). We measured extent of apoptosis in cylindroids using a stain that binds to activated caspase-3. From the accumulation pattern of knockouts in cylindroids, we determined the role of each chemotaxis component on the chemotaxis of *S. typhimurium* toward different tumor regions. The tested strains included three cell surface chemoreceptor knockouts (*tsr, tar*, and *trg*), a flagella knockout (*fla*), a motor assembly knockout (*mot*), and two signal transduction knockouts (*cheA* and *cheY*). The chemoreceptor knockouts are not attracted to serine (*tsr*), aspartate (*tar*), and ribose/galactose (*trg*). The knockouts lacking the flagella (*fla*) and motor assemblies (*mot*) are nonmotile, and knockouts lacking the signal transduction proteins (*cheA* and *cheY*) are motile but do not respond to chemoattractant gradients.

Here, we show that chemotaxis is essential for bacterial accumulation in tumors and that the individual chemoreceptors play essential and independent roles in directing *S. typhimurium* to different microenvironment regions of tumors. Determining the roles of each chemoreceptor and the chemotaxis machinery is an important step in the development of bacterial therapies that are able to target the therapeutically inaccessible regions of tumors. Based on this understanding, novel bacteria strains with improved chemotaxis ability will be developed that can be individually

Requests for reprints: Neil S. Forbes, Department of Chemical Engineering, University of Massachusetts at Amherst, 159 Goessmann Hall, 686 North Pleasant Street, Amherst, MA 01003. Phone: 413-577-0132; Fax: 413-545-1647; E-mail: forbes@ecs.umass.edu.

doi:10.1158/0008-5472.CAN-06-2618

targeted to specific regions of tumors and will be able to overcome the limitations that reduce the efficiency of standard chemotherapies.

Materials and Methods

Bacterial culture. Wild-type (WT; strain SL1344; ref. 17) and all mutant strains of *S. typhimurium* were maintained in Luria broth and on agar plates using standard procedures. For visualization, all strains were transfected with a green fluorescent protein (GFP)-expressing, kanamycin- and ampicillin-resistant plasmid pSMC21 by electroporation with a Gene Pulser (Bio-Rad, Hercules, CA) according to the manufacturer's instructions. Electroporation variables were 1.8 kV, 200-Ω parallel resistance, and 25 μF capacitance.

Three strains of *S. typhimurium* were used to test the role of individual chemoreceptors. Strains ST326, ST328, and ST832 do not possess active *tsr*, *tar*, and *trg* genes, respectively, and were a kind gift from Dr. M. Eisenbach (The Weizmann Institute of Science, Rehovot, Israel; refs. 18, 19). Each chemoreceptor of *S. typhimurium* does not function independently; one of the high-abundance chemoreceptors (Tsr or Tar) must be present to ensure proper functioning of the low-abundance Trg receptor, which has low methyl-accepting activity and limited ability to adapt to stimuli when it is the only receptor present in the cell (20).

Four additional strains of *S. typhimurium* were used to test the role of other components of the chemotaxis machinery. Strains SJW2149 (*fla*), SJW3003 (*mot*), KK2014 (*cheY*), and KK2051 (*cheA*) were obtained from the Salmonella Genetic Stock Centre, University of Calgary (Calgary, Alberta, Canada; refs. 21, 22). Strain SJW2149 (*fla*) does not produce the filament section of the flagella, and strain SJW3003 (*mot*) does not have functioning flagella motors and is incapable of rotating flagella. The enzymes CheA, a histidine kinase, and CheY, a response regulator, are key components of the signal transduction pathway (Fig. 1*A*), which controls bacterial chemotaxis by directing flagellar rotation in response to chemoattractant binding (Fig. 1; refs. 18–20, 23–25). Strain KK2014 (*cheY*) does not possess a functioning CheY protein and rotates its flagella in a counterclockwise direction exclusively, causing the bacteria to run in one direction, independent of chemoattractant gradients (25). Strain KK2051 (*cheA*) does not possess a functioning CheA and cannot regulate the flagella switch, which causes the bacteria to tumble randomly in their environment (24, 26).

Quantification of bacterial chemotaxis with the capillary assay. The ability of the mutant strains to chemotax toward chemoattractant molecules was quantified using the needle-syringe capillary assay developed by Mazumder et al. (27). Cultures of the mutant strains were grown to midlogarithmic phase, centrifuged, washed, and suspended in motility buffer to a final concentration of 3.2×10^7 bacteria/mL (28). Hypodermic needles (25 gauge) attached to 1 mL syringes (Becton Dickinson, Franklin Lakes, NJ) were filled with 0.1 mL of chemoattractant solution containing 0.1 mmol/L serine, 1 mmol/L aspartate, 1 mmol/L ribose, or 1 mmol/L galactose. These concentrations were established by Adler as optimum for chemotaxis (29, 30). The needle-syringe assemblies were inserted into 200 μL pipette tips containing the bacterial suspension and incubated at 35°C for 1 h. After incubation, the content of the needles was removed, diluted, and plated to quantify the number of colony-forming units (CFU). For each strain and each attractant, 27 plates were used. Chemotactic ability, N/N_{Null}, was reported as the ratio of the average number of bacteria that accumulated in the chemoattractant capillaries to the average number of bacteria that accumulated in the chemoattractant-free controls.

Mammalian cell culture. LS174T colon carcinoma cells were grown in DMEM with 10% fetal bovine serum (FBS) and 26 mmol/L HEPES buffer at 37°C and 5% CO_2. Cell aggregates were grown in tissue culture flasks coated with 20 mg/mL poly(2-hydroxyethyl methacrylate) for 9 days to form spheroids.

Cylindroid formation. Formation of tumor cylindroids was done as described previously (1). Briefly, cylindroids were formed by constraining spheroids between the bottom surface of a 96-well plate and the top surface of a set of polycarbonate cylindrical plugs attached to a polycarbonate lid with a gap width of 150 ± 5 μm. The diameter of each cylindroid was dependent on the initial size of the spheroid used in its formation. Spheroids ranging from 150 to 1,000 μm in diameter were selected based on their size, symmetry, and overall integrity. After being constrained, cylindroids were allowed to equilibrate for 22 h in 100 μL DMEM to relieve mechanical stress and establish oxygen and metabolic gradients before subjection to further experimentation (1).

Bacterial inoculation into cylindroids. Before inoculation into cylindroid cultures, all strains were grown at 37°C to midlogarithmic phase (A_{600} 0.3–0.5) from single colony cultures. Individual colonies were chosen from agar plates following confirmation of GFP expression using fluorescence microscopy. Bacterial cultures were centrifuged at 4,000 rpm for 10 min and resuspended in DMEM (Sigma-Aldrich, St. Louis, MO) with 10% FBS (Sigma-Aldrich) and 26 mmol/L HEPES buffer (Invitrogen, Carlsbad, CA) to a final concentration of 500 CFU/mL. Equilibrated cylindroid cultures were inoculated with 100 μL of 500 CFU/mL *S. typhimurium*. Time-lapse fluorescent images were acquired at 10-min intervals up to 34 h after inoculation. Excitation light was shuttered between acquisitions to prevent photobleaching.

To test the influence of aspartate on the behavior of WT *S. typhimurium* accumulation, cylindroids were prepared as described previously, except cylindroids were equilibrated in medium containing 1 or 5 mmol/L of added aspartate. Bacteria added to the cylindroids were suspended in medium containing corresponding concentrations (1 or 5 mmol/L) of aspartate.

Image acquisition and analysis. The accumulation of bacteria and fluorescent dyes in cylindroids was quantified using time-lapse microscopy as described previously (1). An automated stage and image acquisition macro were used to acquire multiple images centered on each cylindroid for multiple days. For each cylindroid, four images (size: 665.8 μm × 873.9 μm) were acquired with a 10× objective and tiled together. Fluorescence intensity inside cylindroids was measured as a function of both position and time. The radius of cylindroids was determined from transmitted light images. Radial profiles were generated from the fluorescent images by averaging all of the pixel intensities at a series of radii from the cylindroid center ($r = 0$) to the cylindroid edge ($r = R$) using a script in ImageJ (NIH Research Services Branch). To account for the effects of autofluorescence, the radial profile at the initial time was subtracted from the profiles.

Analysis of bacterial localization in cylindroid cultures. The chemotactic behavior of the WT and chemoreceptor mutants was quantified by averaging and comparing the fluorescent intensities of different regions in multiple cylindroids. Regions were defined relative to the individual centers and edges of cylindroids. The use of relative distances enabled comparison of multiple cylindroids of different size and the establishment of statistical significance among populations of similar cylindroids.

The growth of the *tar* mutant in cylindroid cultures was determined by measuring the change in fluorescence intensity in the bulk and in the region directly outside the cylindroids as a function of time. For this measurement, the bulk region was defined as a 400 μm^2 area at least 200 μm from the cylindroid edge. The periphery region was defined as an annulus 200 μm in radius around the outside of the cylindroid.

The extent of central accumulation of the *tsr* mutant was quantified by comparing the average fluorescence intensity in the cylindroid center to the intensity at the leading edge of the bacterial ring. The cylindroid center was defined as a circular region with a radius equal to 20% of the cylindroid radius. The bacterial ring was defined as an annulus of pixels with a thickness equal to 20% of the cylindroid radius and centered on the circle of maximum fluorescence intensity. Data were normalized to the maximum pixel intensity of the bulk at the final time point ($t = 26$ h).

The size and location of *trg* colonies in cylindroids were determined using particle analysis in ImageJ. The number of colonies was measured as a function of time, and the location of each colony was determined relative to the center and outside edge of the cylindroids. When counting colonies, a group of two or more bacteria was considered a colony. To exclude single bacterium, the minimum area of an acceptable particle was set at 13 pixels. This value was chosen based on the maximum possible area occupied by two bacteria that are 1.0 μm in diameter and 2.0 μm in length.

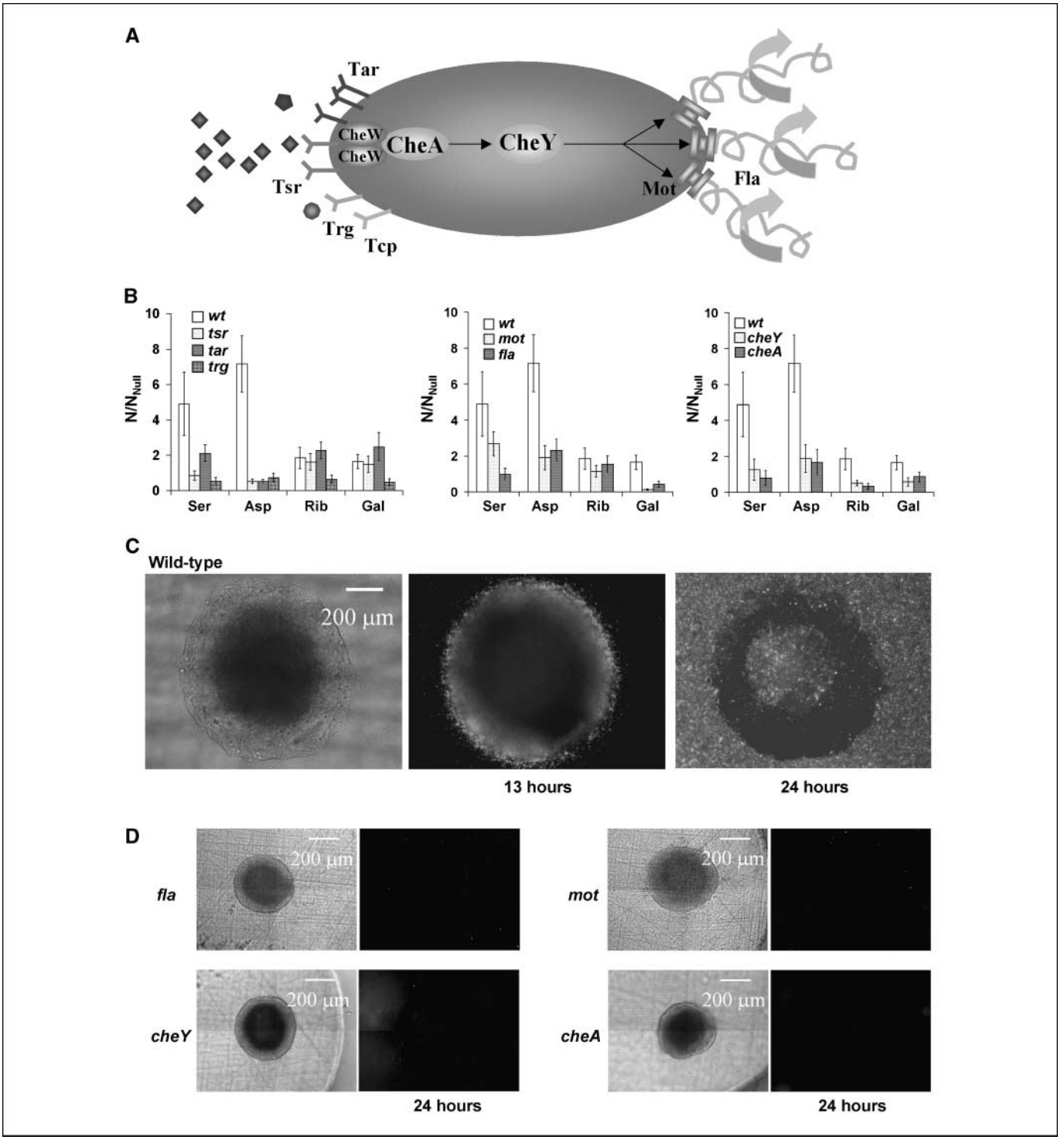

Figure 1. *A,* schematic representation of the chemotaxis machinery of *S. typhimurium*, including four chemoreceptors (Tar, Tsr, Trg, and Tcp), signal transduction proteins (CheW, CheA, and CheY), flagellar motor (Mot), and flagellar assembly (Fla). The enzymes CheA, a histidine kinase, and CheY, a response regulator, control bacterial chemotaxis by directing flagellar rotation in response to chemoattractant binding. When an attractant molecule binds one of the chemoreceptors, the cytoplasmic region of the receptor inhibits autophosphorylation of CheA, which reduces the phosphorylation of CheY. Phosphorylated CheY induces clockwise flagellar rotation and bacterial "tumbling." In an increasing chemoattractant gradient, the concentration of phosphorylated CheY decreases, the frequency of flagella switching decreases, and the bacterium "runs" up the gradient. *B,* chemotactic ability (N/N_{Null}) of the *S. typhimurium* mutants toward serine (*Ser*), aspartate (*Asp*), ribose (*Rib*), and galactose (*Gal*) for the WT and the chemotaxis surface receptor knockouts *tsr, tar*, and *trg*; the nonmotile and flagellated *mot* and the nonflagellated *fla* mutants; and the signal transduction protein knockouts *cheY* and *cheA*. Nine replicate capillary assays were done for each mutant-chemoattractant pair. *C,* accumulation pattern of WT, GFP-expressing *S. typhimurium* in a 930-μm-diameter tumor cylindroid at 13 and 24 h after inoculation. At 13 h, a ring had accumulated at the cylindroid periphery, and at 24 h, bacteria had accumulated in the central necrotic region. *D,* fluorescent microscopy images showing that the following mutants did not accumulate in tumor cylindroids at 24 h after inoculation: a nonflagellated mutant (*fla*; $n = 10$), a nonmotile and flagellated mutant (*mot*; $n = 6$), a *cheY* mutant ($n = 9$), and a *cheA* mutant ($n = 7$). No bacteria were observed chemotaxing toward or accumulating in the cylindroids ($n = 32$).

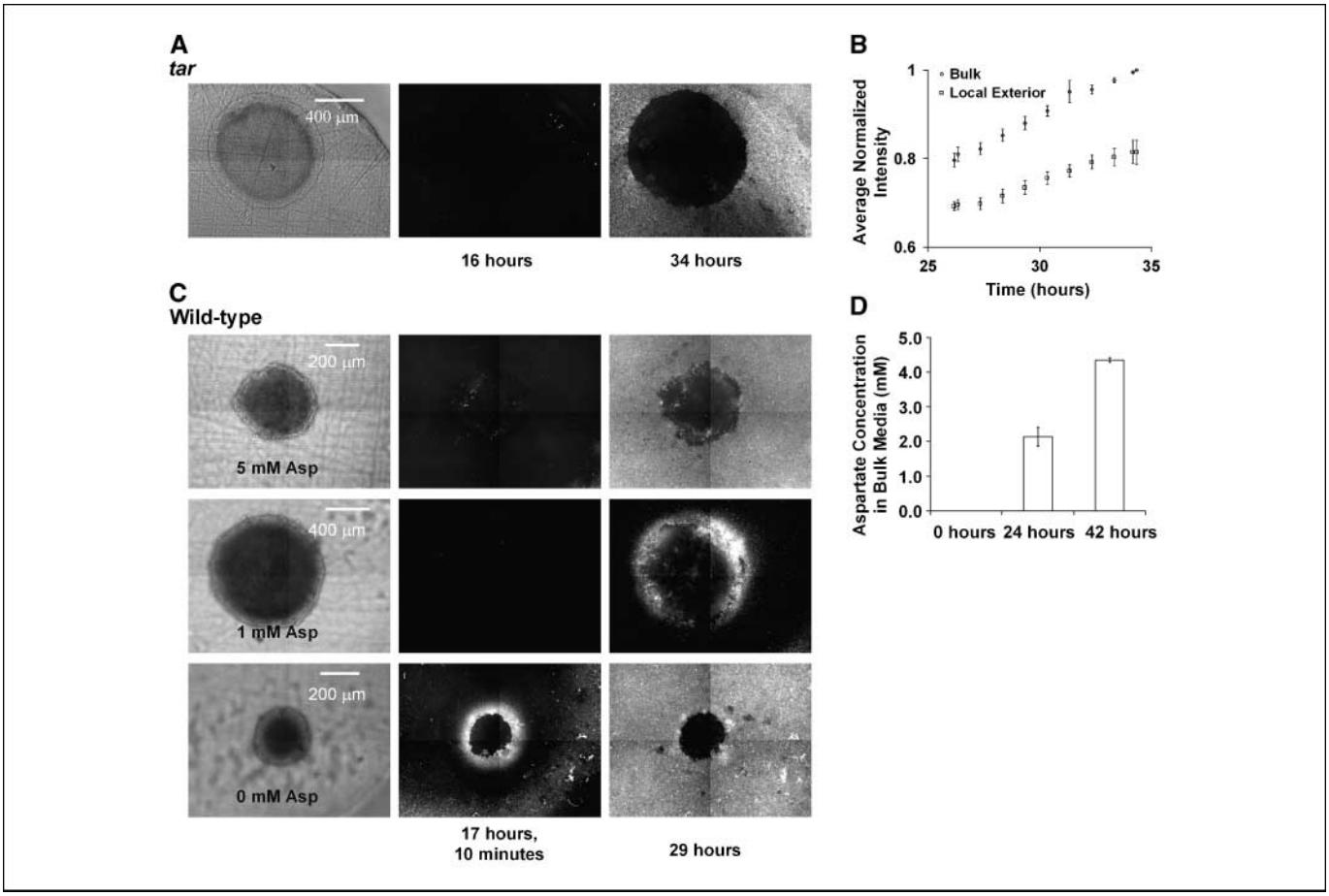

Figure 2. *A,* representative time-lapse fluorescent microscopy images of the accumulation pattern of a *tar* mutant of *S. typhimurium* in a 1,000-μm-diameter tumor cylindroid at 16 and 34 h after inoculation. The bacteria did not form a ring at 16 h and did not accumulate inside the cylindroids at 34 h. *B,* a temporal intensity profile within two regions outside of the cylindroids: a 400 μm^2 area in the bulk >200 μm from the cylindroid edge and an annulus 200 μm thick around the cylindroid edge. Intensities were averaged across multiple cylindroids ($n = 4$). *C,* accumulation pattern of WT *S. typhimurium* in tumor cylindroids with a bulk concentration of 5, 1, and 0 mmol/L of added aspartate at 17 h, 10 min, and 29 h after inoculation. *D,* bulk concentration of aspartate released from colon carcinoma cells in tumor spheroid culture at 0, 24, and 42 h ($n = 3$).

The overall accumulation of each strain was determined by measuring the average pixel intensity inside the cylindroid boundary at 24 h and normalizing to the average pixel intensity of the WT.

Quantification of aspartate produced by spheroids. To quantify the amount of aspartate produced by spheroids, 100 μL samples were taken from three spheroid cultures at 0, 24, and 42 h after changing the medium. Spheroids were grown in spinner flasks to an average diameter of 715 μm and a density of ~20 spheroids/mL. The aspartate concentration was measured according to the method of Christopherson et al. (31). Each sample was lyophilized overnight and dissolved in 100 μL of dimethylformamide and 100 μL of *N*-methyl-*N*-(tert-butyldimethylsilyl) trifluoroacetamide containing 1% tert-butyldimethylchlorosilane at 70°C for 1 h to produce tert-butyldimethylsilyl amino acid derivatives. Gas chromatography-mass spectroscopy analysis was done using an Agilent 6890 with a 30 m × 0.25 mm, 0.25-μm film thickness, DB-5 capillary column (Supelco, Bellefonte, PA) and a Micromass gas chromatography time-of-flight mass spectrometer. The injector temperature, detector temperature, and injection volume were 300°C, 280°C, and 10 μL, respectively (31). The oven temperature was ramped from 140°C to 255°C at 3°C per minute to completely separate metabolites. The relative molar concentration of aspartate in each sample was calculated from standard curves with standards of known concentration.

Quantification of apoptotic cells. The extent of apoptosis was measured in cylindroids using the CaspGLOW Red Caspase-3 Staining kit (BioVision, Inc., Mountain View, CA). This assay uses DEVD-FMK, an inhibitor that irreversibly binds to activated caspase-3, conjugated to sulforhodamine (Red-DEVD-FMK). To stain for apoptotic cells, 100 μL of 1:1,000 (v/v) Red-DEVD-FMK in DMEM was added to each cylindroid-containing well. The cylindroids were incubated in staining solution at 37°C and 5% CO_2 for 2 h. The staining medium was not removed before imaging because it is nontoxic to mammalian cells. The location of apoptosis was determined by generating radial intensity profiles of cells stained with Red-DEVD-FMK. The fluorescence intensity was normalized to the maximum pixel intensity at the final time point (20 h). The average increase in caspase-3 activity was determined by subtracting the average Red-DEVD-FMK intensity throughout the entire cylindroid at 3 h from the average intensity at 20 h after inoculation. The extent of apoptosis induced per individual bacterium was determined by normalizing the average difference in caspase-3 activity at 3 and 20 h by the average bacterial intensity throughout the cylindroids.

Results

Chemotaxis deficiency in mutant *S. typhimurium*. The needle-syringe assay was done with the chemotaxis machinery mutants to determine their relative attraction to the known *S. typhimurium* attractants (Fig. 1*B*). Chemotactic ability is reported as the average number of bacteria in the chemoattractant containing capillaries compared with the average number of bacteria in the control capillaries (N/N_{Null}). A N/N_{Null} ratio of ≤1.0 indicates that bacterial

movement is driven by random motility and not by specific chemotaxis. As expected, the WT was attracted to aspartate, serine, ribose, and galactose, and the chemoreceptor knockouts (*tsr, tar*, and *trg*) were not attracted to their corresponding chemoattractants (serine, aspartate, and ribose/galactose; $P < 0.05$; Fig. 1*B*). The strains with mutations in the flagellar machinery (*mot* and *fla*) and the chemotaxis signal transduction pathway (*cheA* and *cheY*) had decreased chemotactic ability toward all of chemoattractant molecules compared with the WT (Fig. 1*B*), confirming the reported necessity of these proteins for chemotaxis (24).

WT accumulation in cylindroids. The accumulation of each mutant strain in cylindroids was compared with the accumulation of WT *S. typhimurium* as a control. As previously observed, the WT penetrated into the periphery of cylindroids at early times (13 h) and formed a ring of bacteria (Fig. 1*C*; ref. 1). At later times (24 h), bacteria accumulated in the necrotic center of the cylindroids (Fig. 1*C*). During this time, individual *S. typhimurium* were observed through the eyepiece actively swimming toward the central region of the cylindroids (data not shown).

Nonmotile and signal transduction pathway mutants do not chemotax toward cylindroids. The nonmotile (*fla, n* = 10 and *mot, n* = 6) and the signal transduction (*cheY, n* = 9 and *cheA, n* = 7) mutants did not form a discernible ring at the cylindroid periphery throughout the course of growth in cylindroid cultures (Fig. 1*D*), indicating that these mutants are not attracted to cylindroids. Each strain was visibly fluorescent and was observed replicating in the bulk at rates similar to the WT (data not shown). By visual observation under the microscope, it was confirmed that the *cheA* and *cheY* mutants were motile and the *fla* and *mot* mutants were not motile in cylindroid cultures (data not shown).

The aspartate receptor is necessary for *S. typhimurium* chemotaxis toward cylindroids. Presence of the Tar receptor is essential for *S. typhimurium* chemotaxis toward tumor cylindroids (Fig. 2*A*). When inoculated into multiple cylindroids, *tar* did not form a ring at the peripheral edge of cylindroids at any time points ($n = 21$; Fig. 2*A*). At early times (16 h), no accumulation was observed at the cylindroid edge (Fig. 2*A*). At later times (34 h), the concentration of bacteria increased in both the bulk and the peripheral region surrounding the outside of the cylindroids (Fig. 2*A*). The average fluorescence intensity increased as a function of time within these two regions, indicating that bacteria are actively growing in both the local exterior region ($P < 0.01$; $n = 4$) and the bulk ($P < 0.01$; $n = 4$; Fig. 2*B*). The lack of an accumulation ring, which was present following inoculation with the WT (Fig. 1*C*), indicates that *tar* does not chemotax toward cylindroids. Once flooding of the bulk began to occur, individual bacteria were able to chemotax into large tumor cylindroids and accumulate within the centers (data not shown). This suggests that functionalities of the remaining receptors were preserved in this environment.

The addition of aspartate to the bulk medium confirms that the Tar receptor is the dominant receptor governing external chemotaxis of *S. typhimurium* toward tumor cylindroids (Fig. 2*C*). Aspartate was added to the bulk medium to eliminate the gradient at the cylindroid outer edge. The presence of a gradient was confirmed by measuring the concentration of aspartate in the bulk medium of spheroid cultures as a function of time (Fig. 2*D*). Spheroids composed of colon carcinoma cells excrete aspartate at an average rate of 1.0×10^{-13} mmol/cell/h. The inhibition of ring formation by WT *S. typhimurium*, which have functional aspartate

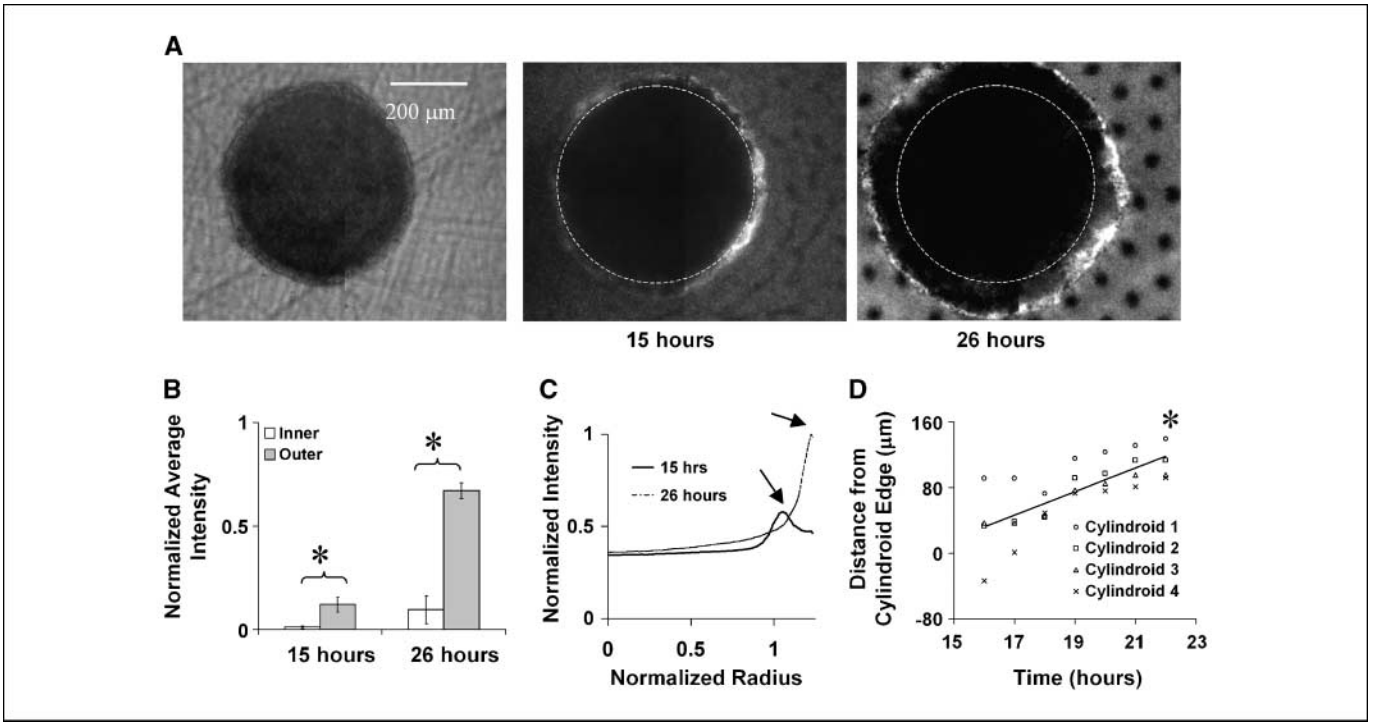

Figure 3. *A,* time-lapse fluorescent microscopy images showing that the *tsr* mutant did not accumulate at the center of tumor cylindroids at 15 and 26 h after inoculation. The ring of bacteria that formed at the edge moved away from the cylindroid with time. *Dashed line,* edge of the cylindroid. *B,* average normalized intensity of bacteria located at the center of the cylindroid (20% of the radius) and within an annulus, 20% thick, inward from the leading edge of the bacterial ring at 15 and 26 h after inoculation. More bacteria were present at the periphery than at the center ($P < 0.01$). *C,* normalized radial intensity profiles corresponding to the images in (*A*). *Arrows,* location of the bacterial ring at 15 and 26 h. *D,* average increase in the radius of the bacterial ring from 16 to 22 h after inoculation ($n = 5$). The rate was statistically non-zero. *, $P < 0.01$.

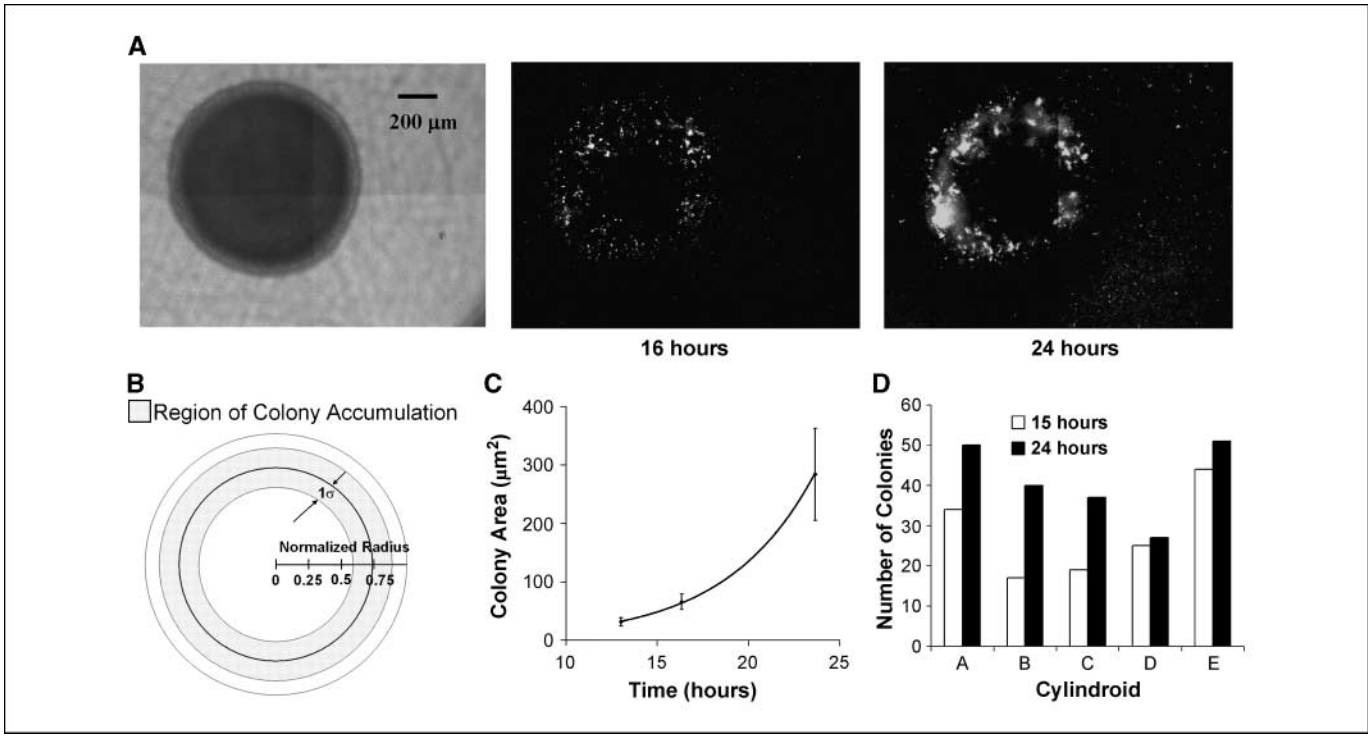

Figure 4. *A,* time-lapse fluorescent microscopy images showing the accumulation pattern of the *trg* mutant in tumor cylindroid at 16 and 22 h after inoculation. *B,* average radial location ($r/R = 0.74 \pm 0.15$) of *trg* colonies depicted in (*A*). *Shaded area,* region 1 SD wide around the mean location of colony formation ($n_{cylindroid} = 4$; $n_{colonies} = 103$). *C,* the area of *trg* colonies increased exponentially with a doubling time of 4.9 min ($n_{cylindroid} = 4$; $n_{colonies} = 396$). *D,* the number of *trg* colonies increased per cylindroid from 15 to 24 h ($n_{cylindroid} = 5$).

receptors, shows that chemotaxis is driven by this aspartate gradient (Fig. 2*C*). When the bulk concentration of aspartate was increased to 5 mmol/L, WT *S. typhimurium* did not form of a ring and did not chemotax toward tumor cylindroids at any time ($n = 10$; Fig. 2*C*). In comparison, the controls (0 mmol/L added aspartate) formed bacterial rings at the edge of the cylindroids within 17 h ($n = 9$; Fig. 2*C*). In the 0 mmol/L controls, individual WT bacteria were observed through the eyepiece actively swimming toward the center of the cylindroids at 17 h (data not shown).

The timing of WT *S. typhimurium* chemotaxis toward cylindroids was dependent on the bulk aspartate concentration. At intermediate aspartate concentrations (1 mmol/L), a chemotactic ring formed after a longer period (29 h; $n = 4$; Fig. 2*C*). This delay suggests that the cancer cells in the cylindroids produced enough aspartate during this time to reestablish a recognizable gradient (Fig. 2*C*) and that the concentration of aspartate at the cylindroid edge was between 1 and 5 mmol/L.

Initiation of *S. typhimurium* penetration into cylindroids is controlled by the Tsr chemoreceptor. The serine receptor mutant *tsr* chemotaxed toward but did not accumulate in the center of tumor cylindroids (Fig. 3) as shown by the formation of a ring of bacteria at the cylindroid edge (Fig. 3*A*). The *tsr* mutant was not observed accumulating in the center of cylindroids up to 30 h after inoculation ($n = 5$; Fig. 3*A*). At early and late time points (15 and 26 h), the average pixel intensity at the center (the internal 20%) of the observed cylindroids was significantly less than the average intensity at the leading edge of the bacterial ring ($P < 0.01$; $n = 5$; Fig. 3*B*). Once the ring of bacteria was established, the bacteria did not move into the cylindroid (Fig. 3*C*). This behavior was different from the WT strain, which possesses functional Tsr receptors, and accumulated in the center of cylindroids (Fig. 1*C*).

At early time points, the *tsr* mutant accumulated at the periphery of cylindroids, creating a ring that moved outward from the cylindroids with time (Fig. 3*A*). Based on the transmitted light images, the radius of the cylindroids did not change throughout the experiments. The cylindroid boundary is indicated by the dashed line in the fluorescence images in Fig. 3*A*. The outward movement of the bacterial ring is reflected in the radial intensity profiles, where the maximum concentration of bacteria at 15 and 26 h was found at $r/R = 1.06$ and $r/R = 1.23$, respectively (Fig. 3*C*), where r/R is the radial position normalized by the radius of the cylindroid. The ring of bacteria moved away from all observed cylindroids at 14.4 ± 2.6 μm/h ($n = 4$; Fig. 3*D*).

Over time, the *tsr* mutant formed a distinct honeycomb pattern in the bulk (Fig. 3*A*), which is caused by self-produced aspartate gradients (32, 33). The outward movement of the bacterial ring and the growth of individual void spaces in *tsr* cultures may have been caused by similar aggregation mechanisms. The local aspartate gradients around *tsr* mutants in the bulk may have been greater than the aspartate gradient produced by tumor cells and appear to have pulled the bacteria from the cylindroids into the bulk (Fig. 3*A*).

Deletion of the Trg receptor induces accumulation in tumor quiescence. Absence of the Trg receptor caused *S. typhimurium* to accumulate in the quiescent region of tumor cylindroids. The *trg* mutant accumulated in distinct colonies within a broad ring between the outer, proliferating edge (Fig. 4*A*) and the central apoptotic region of cylindroids (Fig. 5*A*). Twenty-four hours after inoculation, the average center of mass of each colony was located at $r/R = 0.74 \pm 0.15$ (Fig. 4*B*), which coincides with the location of

quiescent cells in tumor cylindroids (1). Colonies of the *trg* mutant did not accumulate within the central necrotic region ($P < 0.01$). This accumulation pattern was different from the WT strain, which accumulated in the necrotic region of cylindroids between $0 < r/R < 0.4$ (Fig. 1*C*). The difference of these patterns suggests that WT *S. typhimurium*, with active Trg receptors, are attracted to purines and sugars, specifically ribose and galactose, which are released from degraded nuclei in the necrotic center of cylindroids (34).

Within cylindroids, the *trg* colonies increased in size and number over the duration of observation (Fig. 4*A*). The average growth of each colony was exponential with a doubling time of 4.9 h ($n_{\text{colonies}} = 396$; $n_{\text{cylindroids}} = 4$; Fig. 4*C*). This size increase was evidence of bacterial growth within cylindroids. The average number of colonies increased from 28 ± 11 to 41 ± 10 in the cylindroids between 15 and 24 h ($n_{\text{cylindroids}} = 5$; Fig. 4*D*). The increase in colony number is an indication that chemotaxis continued throughout the experiment. In addition, *trg* did not form a ring of bacteria at the periphery of the cylindroids at early time points as observed in the WT (Fig. 1*C*).

Accumulation of *trg* induces apoptosis in tumor cylindroids. Accumulation of the *trg* mutant induced tumor cell apoptosis in cylindroids (Fig. 5). The *trg* mutant localized to the expanding front of apoptotic cells in cylindroids (Fig. 5*A*). The activity of caspase-3, a mediator of mammalian cell apoptosis, increased between 3 and 20 h after inoculation with *trg* ($n = 6$ per group; Fig. 5*B*). The extent of apoptosis increased more in the center of cylindroids than at the edge (Fig. 5*B*). The average increase of caspase-3 activity was significantly greater for both the WT and *trg* compared with untreated controls ($P < 0.05$; $n = 6$ per group; Fig. 5*C*). Compared with the WT, fewer bacteria accumulated in cylindroids inoculated with *trg*. When the caspase-3 activity was normalized by the average bacterial intensity, *trg* induced significantly more tumor cell apoptosis per bacterium than the WT ($P < 0.05$; $n = 6$; Fig. 5*D*). This difference between *trg* and the WT suggests that *S. typhimurium* strains that target quiescent regions of tumors will have an increased therapeutic effect over strains that preferentially colonize tumor necrosis.

Overall internal accumulation of all Salmonella strains. To assess the overall extent of accumulation for each strain into tumor cylindroids, the average pixel intensity per area of cylindroid was calculated ($n_{\text{cylindroid}} = 24$; Fig. 6*A*). The average pixel intensity represents the average bacterial concentration throughout the cylindroids at 24 h. The WT accumulated in cylindroids significantly more than any other strain ($P < 0.05$). The *trg* and *tsr* mutants accumulated half and one tenth of the accumulation of the WT, respectively ($P < 0.01$). The remaining mutant strains did not accumulate inside the tumor cylindroid at significant concentrations ($P < 0.01$).

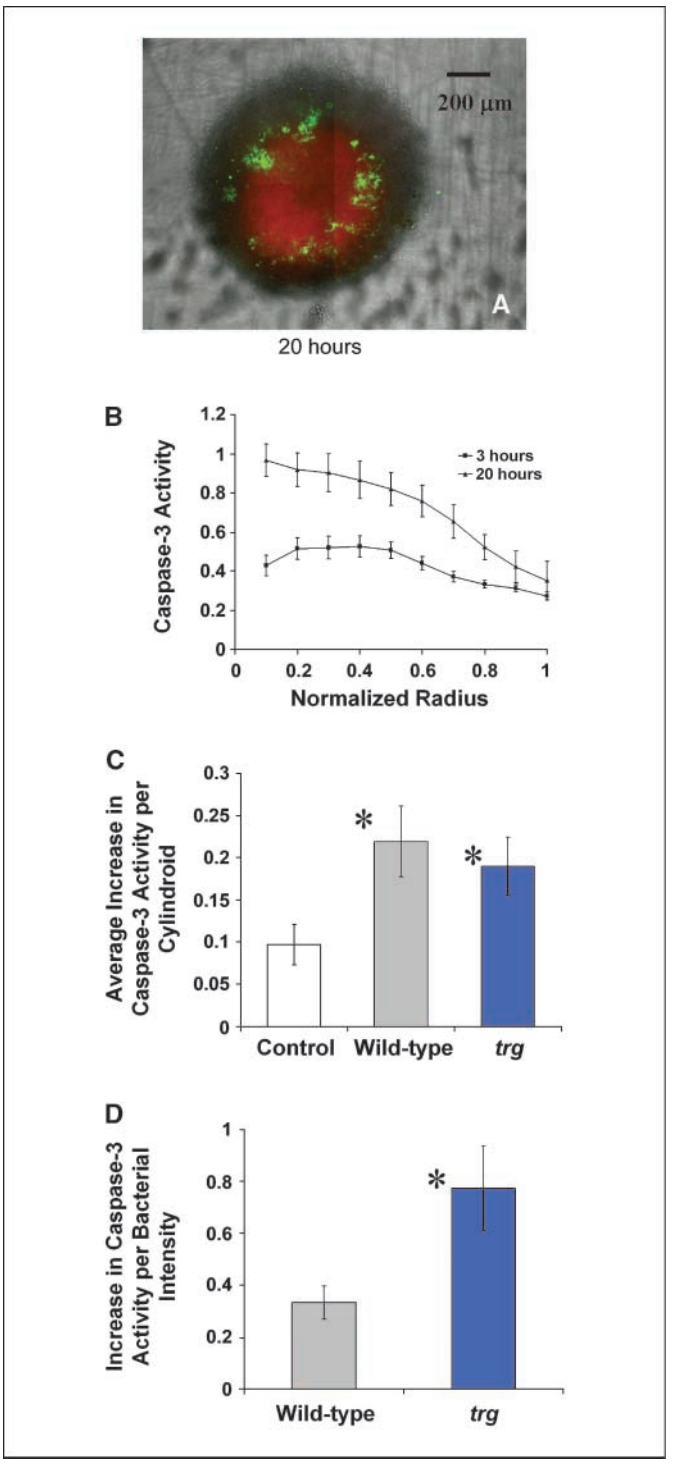

Figure 5. *A,* fluorescent microscopy image showing the extent and location of *trg* accumulation (*green*) and the extent of apoptosis (*red*) in a tumor cylindroid 20 h after inoculation. The extent of apoptosis was detected using sulforhodamine conjugated to DEVD-FMK, a caspase-3 inhibitor that irreversibly binds to activated caspase-3 in apoptotic cells. *B,* fluorescence radial intensity profile showing the increase in caspase-3 expression in cylindroids between 3 and 20 h after inoculation with the *trg* mutant ($n = 6$). Caspase-3 expression increased more in the center of cylindroids than at the edge. *C,* the average increase in caspase-3 activity per cylindroid was significantly greater for the WT and *trg* mutant than untreated controls ($n = 6$). *, $P < 0.05$. *D,* the increase in caspase-3 activity normalized by the bacterial intensity was significantly greater for the *trg* mutants compared with the WT ($n = 6$). *, $P < 0.05$.

Discussion

Each component of the chemotaxis machinery was necessary for accumulation of *S. typhimurium* in tumor cylindroids, and each chemoreceptor directs *S. typhimurium* to different microenvironments within tumors. The Tar receptor caused migration of *S. typhimurium* to the edge of cylindroids, the Tsr receptor initiated penetration into cylindroids, and the Trg receptor directed *S. typhimurium* toward necrosis (Fig. 6*B*).

The signal transduction pathway and flagella machinery are necessary for chemotaxis toward tumor cylindroids. Chemotaxis was essential for accumulation of *S. typhimurium* in tumor

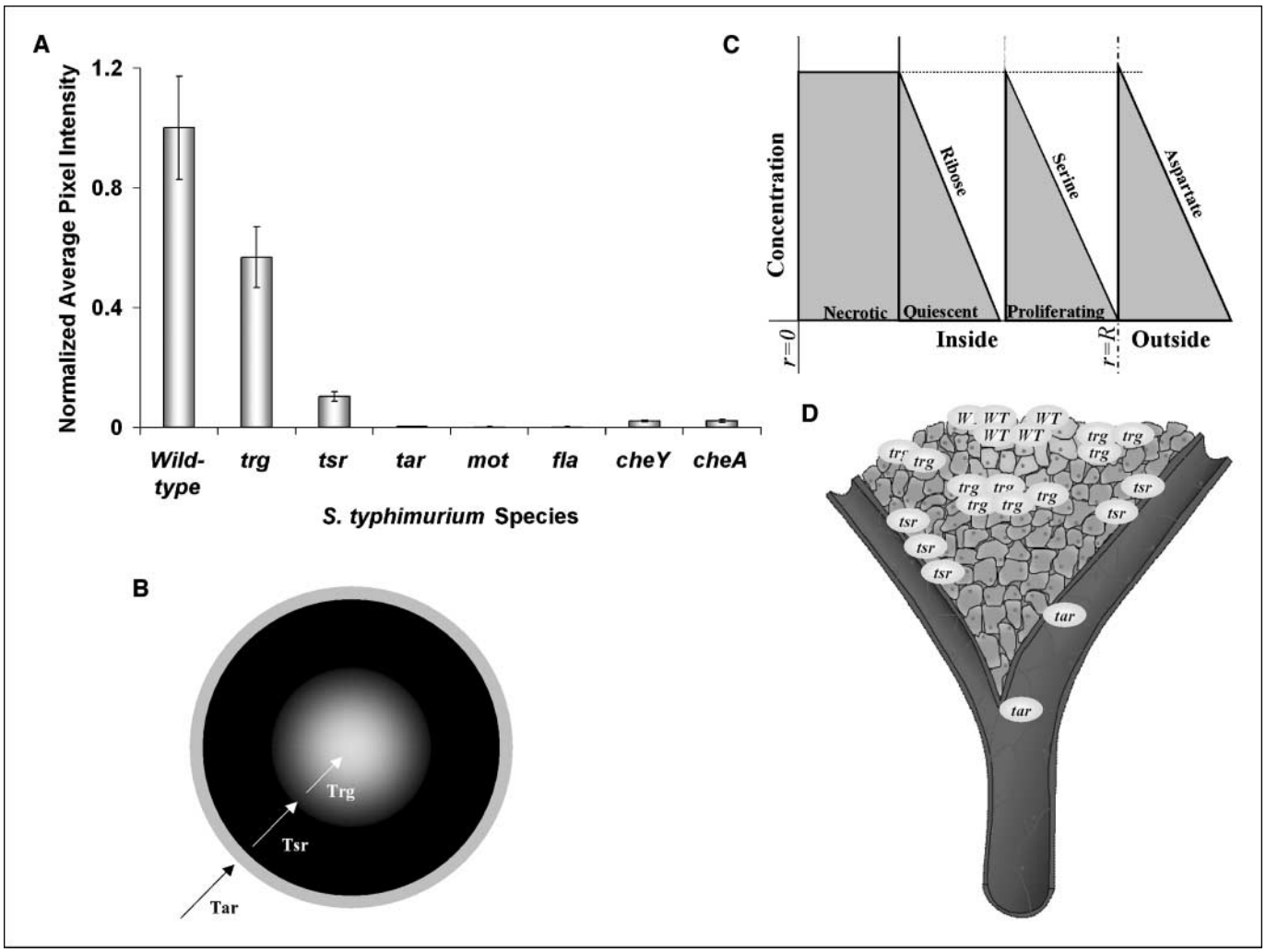

Figure 6. *A,* total internal accumulation of all individual species of mutant *S. typhimurium* in tumor cylindroids at 24 h after inoculation ($n = 3$). *B,* schematic representation of the individual roles of the chemoreceptors on chemotaxis and accumulation in tumor cylindroids. *C,* suggested chemoattractant gradient profiles located in tumor cylindroids that contain necrotic, quiescent, and proliferative regions. All concentrations are shown normalized to a maximum value inside cylindroids. *D,* projected accumulation pattern of WT and receptor knockouts (*tar, tsr*, and *trg*) *S. typhimurium* in heterogeneous tumor tissue surrounding a branched blood vessel. The *tar* mutant will remain in the blood vessel, the *tsr* mutant will not penetrate in the tumor tissue, the WT will accumulate in the necrotic region, and the *trg* mutant will accumulate in colonies within the quiescent region.

cylindroids. General motility and properly constructed flagella were necessary for accumulation within tumor cylindroids (Fig. 1*D*). In the nonmotile mutants *mot* and *fla*, signals are correctly transmitted from the receptors through the cytoplasmic signal proteins, but improper functioning of the motor or lack of flagella filament prevents the bacteria from swimming up attractant gradients. Lack of accumulation in tumor cylindroids by these nonmotile mutants showed that chemotaxis, and not selective growth, is necessary to promote accumulation in tumors.

Complete functioning of the signal transduction pathway was also required for accumulation of *S. typhimurium* in tumor cylindroids (Fig. 1*D*). Without functioning signal transduction proteins (CheY and CheA), bacteria are motile but movement is not directed by attraction to chemoattractants (Fig. 1*D*; ref. 35). In the presence of an attractant gradient, the receptors bind attractant molecules, but a signal is not transmitted to the flagella (Fig. 1*A*) and the bacteria move randomly. The lack of accumulation of *cheY* and *cheA* showed that random bacterial motion did not contribute to *S. typhimurium* accumulation in tumor cylindroids.

Chemoreceptors direct the accumulation of *S. typhimurium* toward specific microenvironments in tumors. Each chemoreceptor played a specific role in the chemotaxis of *S. typhimurium* in tumor cylindroids (Fig. 6*B*), and the accumulation pattern of each mutant suggests where chemoattractant gradients exist in cylindroids (Fig. 6*C*). Presence of the aspartate receptor was necessary for external chemotaxis toward tumor cylindroids, the serine receptor was necessary to initiate internal colonization of tumor cylindroids, and the ribose/galactose receptor directed bacteria into the central necrotic core of cylindroids (Fig. 6*B*). Results with the chemoreceptor knockouts further suggest that (*a*) an external aspartate gradient was present at the edge of cylindroids that attracted *S. typhimurium* to cylindroids, (*b*) a serine gradient existed in the cylindroid periphery that directed *S. typhimurium* penetration into cylindroids, and (*c*) a ribose/galactose gradient existed around the cylindroid center that attracted *S. typhimurium* into the necrotic core (Fig. 6*C*). The *tar* mutant, which has functional Tsr and Trg receptors, did not chemotax toward tumor cylindroids (Fig. 2), suggesting that

neither a serine nor a ribose/galactose gradient existed away from the cylindroid edge into the bulk (Fig. 6*C*). The inability of *tsr*, which contains functional Trg receptors, to accumulate within cylindroids (Figs. 3 and 6*A*) suggests that a ribose/galactose gradient did not exist at the periphery of cylindroids (Fig. 6*C*). The lack of central accumulation of the *trg* mutant (Fig. 5*A*) suggests that a ribose or galactose gradient existed around the cylindroid center, which may have been the result of the nuclear degradation of necrotic cells (Fig. 6*C*).

The interaction of the components of the chemotaxis machinery with chemoattractant gradients in cylindroids suggests how mutant *S. typhimurium* would accumulate in tumors *in vivo*. Because cancer cells grown as spheroids produced and excreted aspartate (Fig. 2*D*), an aspartate gradient may exist at the blood vessel lumen bordering *in vivo* tumors. In this environment, the *tar* mutant would not be attracted to a tumor and would remain in the blood vessel (Fig. 6*D*). Based on the chemoattractant gradients present in cylindroids (Fig. 6*C*), migration of *S. typhimurium* from blood vessels into tumors would be initiated by the Tsr receptor and accumulation in necrotic regions would be directed by the Trg receptor (Fig. 6*D*). A *tsr* mutant would remain in the tumor periphery, WT *S. typhimurium* would accumulate in necrotic regions, and a *trg* mutant would accumulate in quiescent regions (Fig. 6*D*).

Control of bacterial accumulation in tumors could be achieved by selectively eliminating chemoreceptor genes from therapeutic *S. typhimurium* strains. The *trg* mutant is particularly promising because it accumulated in the therapeutically inaccessible, quiescent region of cylindroids and showed a greater individual effect on inducing apoptosis than the WT. This mutant is attracted to tumors, can penetrate into tumor tissue, but does not preferentially colonize tumor necrosis. By genetically manipulating the behavior of the *trg* mutant, new strains of *S. typhimurium* could be created that more effectively colonize the quiescent regions of tumors that are otherwise unaffected by standard cancer therapeutics.

Acknowledgments

Received 7/17/2006; revised 12/4/2006; accepted 1/18/2007.

Grant support: Susan G. Komen Breast Cancer Foundation grant BCTR0601001 and Collaborative Biomedical Research Program at the University of Massachusetts, Amherst.

The costs of publication of this article were defrayed in part by the payment of page charges. This article must therefore be hereby marked *advertisement* in accordance with 18 U.S.C. Section 1734 solely to indicate this fact.

We thank Dr. M. Eisenbach for the kind gift of the receptor knockout *S. typhimurium* strains *tar, trg*, and *tsr*.

References

1. Kasinskas RW, Forbes NS. *Salmonella typhimurium* specifically chemotax and proliferate in heterogeneous tumor tissue *in vitro*. Biotechnol Bioeng 2006;94:710–21.
2. Parker RC, Plummer HC, Siebenmann CO, Chapman MG. Effect of histolyticus infection and toxin on transplantable mouse tumors. Proc Soc Exp Biol Med 1947;66:461–7.
3. Pawelek JM, Low KB, Bermudes D. Tumor-targeted Salmonella as a novel anticancer vector. Cancer Res 1997;57:4537–44.
4. Jain RK, Forbes NS. Can engineered bacteria help control cancer? Proc Natl Acad Sci U S A 2001;98:14748–50.
5. Forbes NS, Munn LL, Fukumura D, Jain RK. Sparse initial entrapment of systemically injected *Salmonella typhimurium* leads to heterogeneous accumulation within tumors. Cancer Res 2003;63:5188–93.
6. Giaccia AJ. Hypoxic stress proteins: survival of the fittest. Semin Radiat Oncol 1996;6:46–58.
7. Kim JJ, Tannock IF. Repopulation of cancer cells during therapy: an important cause of treatment failure. Nat Rev Cancer 2005;5:516–25.
8. Minchinton AI, Tannock IF. Drug penetration in solid tumours. Nat Rev Cancer 2006;6:583–92.
9. Clairmont C, Lee KC, Pike J, et al. Biodistribution and genetic stability of the novel antitumor agent VNP20009, a genetically modified strain of *Salmonella typhimurium*. J Infect Dis 2000;181:1996–2002.
10. Low KB, Ittensohn M, Le T, et al. Lipid A mutant Salmonella with suppressed virulence and TNFα induction retain tumor-targeting *in vivo*. Nat Biotechnol 1999;17:37–41.
11. Low KB, Ittensohn M, Luo X, et al. Construction of VNP20009: a novel, genetically stable antibiotic-sensitive strain of tumor-targeting Salmonella for parenteral administration in humans. Methods Mol Med 2004;90:47–60.
12. Luo X, Li Z, Lin S, et al. Antitumor effect of VNP20009, an attenuated Salmonella, in murine tumor models. Oncol Res 2000;12:501–8.
13. Yu YA, Shabahang S, Timiryasova TM, et al. Visualization of tumors and metastases in live animals with bacteria and vaccinia virus encoding light-emitting proteins. Nat Biotechnol 2004;22:313–20.
14. Mei S, Theys J, Landuyt W, Anne J, Lambin P. Optimization of tumor-targeted gene delivery by engineered attenuated *Salmonella typhimurium*. Anticancer Res 2002;22:3261–6.
15. Zhao M, Yang M, Li XM, et al. Tumor-targeting bacterial therapy with amino acid auxotrophs of GFP-expressing *Salmonella typhimurium*. Proc Natl Acad Sci U S A 2005;102:755–60.
16. Zhao M, Yang M, Ma H, et al. Targeted therapy with a *Salmonella typhimurium* leucine-arginine auxotroph cures orthotopic human breast tumors in nude mice. Cancer Res 2006;66:7647–52.
17. Aswad D, Koshland DE, Jr. Isolation, characterization, and complementation of *Salmonella typhimurium* chemotaxis mutants. J Mol Biol 1975;97:225–35.
18. Blat Y, Eisenbach M. Tar-dependent and -independent pattern formation by *Salmonella typhimurium*. J Bacteriol 1995;177:1683–91.
19. Clarke S, Koshland DE, Jr. Membrane receptors for aspartate and serine in bacterial chemotaxis. J Biol Chem 1979;254:9695–702.
20. Barnakov AN, Barnakova LA, Hazelbauer GL. Comparison *in vitro* of a high- and a low-abundance chemoreceptor of *Escherichia coli*: similar kinase activation but different methyl-accepting activities. J Bacteriol 1998;180:6713–8.
21. Ohnishi K, Ohto Y, Aizawa S, Macnab RM, Iino T. FlgD is a scaffolding protein needed for flagellar hook assembly in *Salmonella typhimurium*. J Bacteriol 1994;176:2272–81.
22. Yamaguchi S, Fujita H, Taira T, et al. Genetic analysis of three additional fla genes in *Salmonella typhimurium*. J Gen Microbiol 1984;130:3339–42.
23. Adler J. Chemoreceptors in bacteria. Science 1969;166:1588–97.
24. Borkovich KA, Kaplan N, Hess JF, Simon MI. Transmembrane signal transduction in bacterial chemotaxis involves ligand-dependent activation of phosphate group transfer. Proc Natl Acad Sci U S A 1989;86:1208–12.
25. Wolfe AJ, Conley MP, Kramer TJ, Berg HC. Reconstitution of signaling in bacterial chemotaxis. J Bacteriol 1987;169:1878–85.
26. Wylie D, Stock A, Wong CY, Stock J. Sensory transduction in bacterial chemotaxis involves phosphotransfer between Che proteins. Biochem Biophys Res Commun 1988;151:891–6.
27. Mazumder R, Phelps TJ, Krieg NR, Benoit RE. Determining chemotactic responses by two subsurface microaerophiles using a simplified capillary assay method. J Microbiol Methods 1999;37:255–63.
28. Adler J, Templeton B. The effect of environmental conditions on the motility of *Escherichia coli*. J Gen Microbiol 1967;46:175–84.
29. Mesibov R, Ordal GW, Adler J. The range of attractant concentrations for bacterial chemotaxis and the threshold and size of response over this range. Weber law and related phenomena. J Gen Physiol 1973;62:203–23.
30. Adler J, Dahl MM. A method for measuring the motility of bacteria and for comparing random and non-random motility. J Gen Microbiol 1967;46:161–73.
31. Early RJ, Thompson JR, Sedgwick GW, Kelly JM, Christopherson RJ. Capillary gas chromatographic analysis of amino acids in blood and protein hydrolysates as tert.-butyldimethylsilyl derivatives. J Chromatogr 1987;416:15–23.
32. Woodward DE, Tyson R, Myerscough MR, et al. Spatio-temporal patterns generated by *Salmonella typhimurium*. Biophys J 1995;68:2181–9.
33. Brenner MP, Levitov LS, Budrene EO. Physical mechanisms for chemotactic pattern formation by bacteria. Biophys J 1998;74:1677–93.
34. Theys J, Barbe S, Landuyt W, et al. Tumor-specific gene delivery using genetically engineered bacteria. Curr Gene Ther 2003;3:207–21.
35. Grebe TW, Stock J. Bacterial chemotaxis: the five sensors of a bacterium. Curr Biol 1998;8:R154–7.

Salmonella typhimurium Lacking Ribose Chemoreceptors Localize in Tumor Quiescence and Induce Apoptosis

Rachel W. Kasinskas and Neil S. Forbes

Cancer Res 2007;67:3201-3209.